# Signature of the transversal coherence length in high-order harmonic generation

C. Hernández-García,* I. J. Sola, and L. Plaja
*Grupo de Investigación en Óptica Extrema, Universidad de Salamanca, E-37008, Salamanca, Spain*
(Received 14 January 2013; published 31 October 2013)

It is well known that high-order harmonic generation (HHG) from extended targets differs substantially from that of isolated atoms. Phase matching during propagation plays a major role in defining the extent of the spatial regions in the target that contribute constructively to the final yield. Typically, the understanding of this process is simplified by considering phase-matching effects along the field propagation axis, defining a longitudinal coherence length. In this paper we explore the role of phase matching in the transverse direction. The definition of a transversal coherence length appears fundamental to understanding propagation of harmonics generated by focalized laser beams. We present experimental results—-supported by theory—in which transversal phase matching plays the leading role in the macroscopic HHG.

DOI: 10.1103/PhysRevA.88.043848 PACS number(s): 42.50.Ar, 42.65.Ky

## I. INTRODUCTION

For intense-field interactions, high-energy photons are generated by high-order harmonic generation (HHG). The underlying mechanism is understood in terms of the three-step model [1,2], in which an electron is first removed from the atom by the laser field and then driven back to the parent ion when the sign of the field reverses. Upon rescattering, the electron can recombine, releasing its kinetic energy in the form of high-order harmonic radiation. The particular properties of the harmonic radiation can be well understood in semiclassical terms [3]. Typically, in each half-cycle there are two possible electron trajectories leading to the same kinetic energy at recollision and, therefore, two possible semiclassical paths for the generation of the same harmonic (each named accordingly to the excursion time as *short* and *long* trajectory). The interference of these two electron paths modifies the efficiency of harmonic generation at the single-atom level. The signature of this quantum path interference (QPI) has been demonstrated to survive in macroscopic targets and to produce modulations in the harmonic yield as the intensity of the driving field is increased [4].

However, harmonic generation in extensive targets can be intricate, as it depends not only on the single-atom response, but also on how the harmonics from these elementary radiators interfere. During propagation, harmonic phase matching also plays an essential role, limiting spatially the regions in which the generated harmonics contribute efficiently [5–8]. Typically, phase matching is described in terms of a longitudinal coherence length, which corresponds to the distance between two atoms whose emitted radiation interferes destructively, being a critical parameter for the optimization of harmonic generation in macroscopic targets. However, it is also possible to define a transversal coherence length in terms of the radiation coming from atoms placed in a plane perpendicular to the propagation axis. Here we look at conditions in which the transversal coherence length is more relevant than the longitudinal. For this, we analyze theoretically and experimentally the effect of an apertured laser beam in the HHG process driven in argon.

We have divided the paper into five sections. In Sec. II, we present the concept of transverse coherence length. In Sec. III we introduce the spatial maps of the harmonic detection as a tool for the analysis of HHG. In Sec. IV, we present experimental and theoretical results for HHG driven by apertured laser beams in a gas jet. For that purpose we have used a 100-fs Ti:Sa laser system (Spectra Physics; 800 nm, 10 Hz, and up to 50 mJ pulse energy) belonging to the laser facility at the University of Salamanca. With the aid of the spatial maps we identify the signature of the transversal coherence length in both theory and experiments. Finally, we conclude in Sec. V.

## II. TRANSVERSAL AND LONGITUDINAL PHASE MATCHING

Let us first develop the concept of longitudinal and transversal phase matching. Considering a detector at some distance $\mathbf{r}_d$, the contribution to the detected harmonic field of an atom located at $\mathbf{r}$ is given by

$$E_q(\mathbf{r}) \propto \left[\left|d_q^s(\mathbf{r})\right|e^{i\phi_q^s(\mathbf{r})} + \left|d_q^l(\mathbf{r})\right|e^{i\phi_q^l(\mathbf{r})}\right]e^{i(\mathbf{r}_d-\mathbf{r})\cdot\mathbf{k}_q}, \quad (1)$$

where $|d_q^j(\mathbf{r})|$ is the spectral amplitude of the single-atom dipole and $\phi_q^j(\mathbf{r})$ its phase, for the long and short contributions ($j = l$ and $j = s$, respectively), and $\mathbf{k}_q$ is the propagation vector [$|k_q| = n(q\omega)q\omega/c$, $\omega$ being the frequency of the driving field and $n(\omega)$ the refractive index].

Assuming a driving field propagating along the $z$ axis, the phase mismatch associated with each trajectory contribution for on-axis detection is defined as

$$\Delta\mathbf{k}_q^j = \mathbf{k}_q - \nabla\phi_q^j = k_q\mathbf{e_z} - \frac{\partial\phi_q^j}{\partial z}\mathbf{e_z} - \frac{\partial\phi_q^j}{\partial\rho}\mathbf{e}_\rho. \quad (2)$$

We can now decompose the phase mismatch into longitudinal ($\Delta k_q^{\parallel}$) and transversal components ($\Delta k_q^{\perp}$) as

$$\Delta k_q^{\parallel} = k_q\mathbf{e_z} - \frac{\partial\phi_q}{\partial z}\mathbf{e_z}, \quad (3)$$

$$\Delta k_q^{\perp} = -\frac{\partial\phi_q}{\partial\rho}\mathbf{e}_\rho \quad (4)$$

*Present address: JILA and Department of Physics, University of Colorado at Boulder, Boulder, Colorado 80309-0440, USA; carloshergar@usal.es

 

and define the longitudinal coherence length as $L_{\rm coh}^{\parallel} = \pi/\Delta k_q^{\parallel}$ and the transversal coherence length, $L_{\rm coh}^{\perp} = \pi/\Delta k_q^{\perp}$.

Let us now consider a Gaussian beam driving field propagating through a medium of refractive index $n(\omega)$. There are different physical contributions to the dipole spectral phase $\phi_q^j(z)$. On one side there is an *extrinsic* contribution originated by the change in phase of the driving field as it propagates (Gouy phase, transversal phase, and dephase due to the presence of free charges and neutrals in the target, included in the refraction index). This extrinsic contribution is independent of the nature of the quantum path involved. On the other hand, there is an *intrinsic* contribution to the dipole phase originated by the single-atom harmonic generation, which depends on the nature of the trajectory ($j$) involved and can be approximated as $\phi_{\rm int}^j \simeq -\alpha^j I$. That phase is proportional to the laser pulse intensity ($I$) by the factor $\alpha_q^j$, which depends on the trajectory, being higher for long ones, ($\alpha_q^l > \alpha_q^s$) [9].

Therefore we can express the longitudinal phase mismatch as

$$\Delta k_q^{\parallel} \simeq q\frac{\omega}{c}\left[n(q\omega) - n(\omega)\right] + (q-1)\frac{\partial \zeta(z)}{\partial z} + \alpha_q^j \frac{\partial I}{\partial z}, \quad (5)$$

where $\zeta(z)$ is the Gouy phase. At low densities at which the effect of the refraction index can be neglected, there are mainly two contributions to the longitudinal phase mismatch: the variation of the Gouy phase, which always decreases with the distance; and the variation of the intrinsic phase, which depends on the intensity gradient, symmetric with respect to the laser focal point. Therefore, the phase mismatch from the Gouy phase is always positive, while that coming from the intrinsic phase changes from positive to negative at the focus. As a consequence, when the target is located after the focus, the opposite behavior of the intrinsic and Gouy phases compensates [10] and results in an efficient longitudinal phase matching [6,11,12].

On the other hand, the transversal phase mismatch is given by

$$\Delta k_q^{\perp} \simeq -q\frac{\omega}{c} n(\omega)\frac{\rho}{R(z)} + \alpha_q^j \frac{\partial I}{\partial \rho}, \quad (6)$$

where $R(z)$ is the radius of curvature of the Gaussian beam wavefront. For low-density gases, there are mainly two contributions to the transversal phase mismatch: the variation of the transversal phase and that of the intrinsic phase. Both contributions are symmetric in the transversal plane. However, the sign of the transversal phase depends on the radius of curvature, therefore it is positive before the focus but negative after the focus position. As a consequence, when the target is located before the focus, the opposite behavior of the intrinsic and transversal phases compensates, thus obtaining favorable transversal phase-matching conditions. Most notably, this behavior is the opposite for the longitudinal coherence length, where it is known to be optimal after the focus rather than before it.

Note, therefore, that the efficiency of the detected signal will depend on the compromise between longitudinal and transversal phase-matching conditions, which behave oppositely with respect to the focus position; i.e., the longitudinal coherence length is longer after the focus, while the transversal coherence length is longer before the focus.

## III. SPATIAL MAPS OF THE HARMONIC DETECTION

We compute harmonic propagation using a method based on the application of the electromagnetic-field propagator [13], instead of the standard numerical solution of the wave equation [14,15]. Every point in the target is treated as the source of an elementary wave, which is then propagated to the detector. The final field at the detector is, thus, the coherent addition of these elementary contributions. One of the advantages of this method is that it allows us to analyze the topology of the harmonic generation, i.e., the contribution of the different target regions to the far-field phase and amplitude of the harmonic at the detector. Here we use this possibility to generate maps of the amplitude and phase of these regions of the target to the total harmonic field at the detector. More information on this method and the SFA+ model used to compute the single-atom harmonic generation may be found in Refs. [16–18].

Let us discuss briefly the information provided by the harmonic generation maps. For this, we focus first on the maps corresponding to the 19th harmonic for a hydrogen gas jet, since, for this element, the harmonic absorption is negligible. Figure 1 shows the cases of the gas jet located 2 mm before [Fig. 1(b)] and after [Fig. 1(c)] the focus position. The laser pulse is assumed to be a $\sin^2$ envelope of 2.9 cycles FWHM (7.7 fs), 800-nm wavelength, and a peak intensity of $1.57 \times 10^{14}$ W/cm$^2$. We have assumed a Gaussian beam (with waist $W_0 = 30$ $\mu$m) focused into a hydrogen gas jet. The gas jet, directed along the $x$ axis (perpendicular to the field propagation), is modeled by a Gaussian distribution along the $y$ and $z$ dimensions (whose FWHM is 500 $\mu$m) and a constant profile along its axial dimension, $x$. The spatial map shows a background color which represents the amplitude of the local contribution to the harmonic far field at the detector, which in this case is located on-axis. This local contribution is obtained by computing the single-atom HHG weighted by the local atom density, and multiplied by the cylindrical volume element, thus assuming cylindrical symmetry of the target. Note that the low contribution at a radius close to 0 is a consequence of the $\rho$ dependence of the cylindrical volume element. On the other hand, the arrows correspond to the polar representation of the field phase. Note that these maps are conceptually different from those presented in Refs. [11,19], in which the background represents the local phase mismatch and the arrows represent the direction in which the harmonic emission is better phase matched.

From our maps, it is possible to identify the longitudinal and transversal coherence length as the spatial distance between phase arrows of opposite direction in the horizontal and vertical directions, respectively. We represent these lengths as horizontal and vertical arrows. We observe that the longitudinal coherence length is larger when the gas jet is placed after the focus position, resulting from the compensation of the Gouy and intrinsic phase, as explained above. On the other hand, in the transversal direction, the compensation of the transversal phase and the intrinsic phase leads to a very large transversal coherence length before the focus (white arrow not shown in this case), while a finite transversal coherence length can be identified after the focus position.

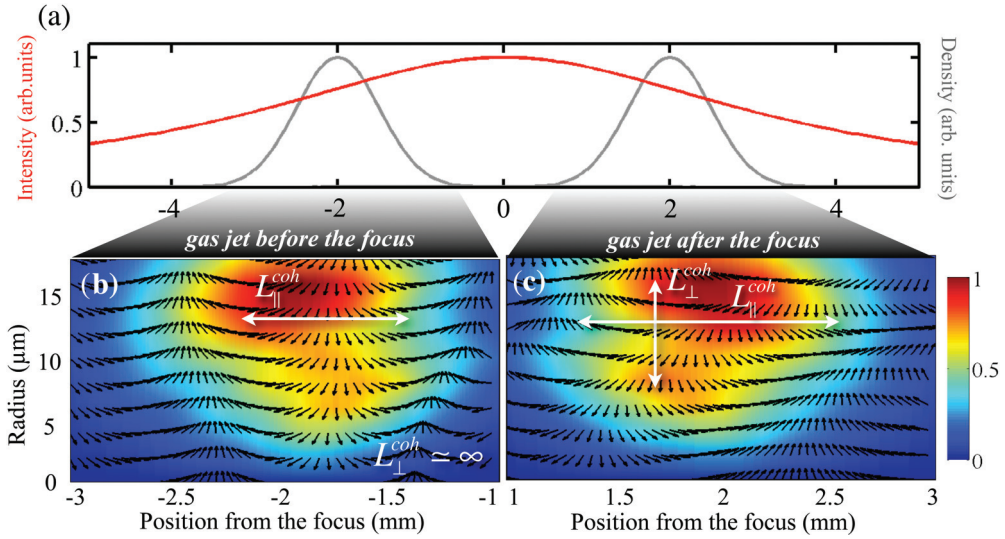


FIG. 1. (Color online) Spatial maps of the harmonic detection for the 19th harmonic for a hydrogen gas jet placed (b) 2 mm before and (c) after the focus position. We assume cylindrical symmetry, therefore each point on the map corresponds to the contribution of a ring at the target with a particular radius and located at a given distance from the focus. The colored background represents the amplitude of the contribution, while the phase is represented by the angle of the titled arrows. (a) The intensity of the fundamental Gaussian beam [smooth (red) line] and the gas density distribution [humped (gray) line] at the two positions presented here. The laser pulse is assumed to be a $\sin^2$ envelope of 2.9-cycle FWHM (7.7 fs), 800-nm wavelength, and a peak intensity of $1.57 \times 10^{14}$ W/cm$^2$. We have assumed a Gaussian beam (with waist $W_0 = 30$ $\mu$m) focused on a hydrogen gas jet of density $10^{18}$ atoms/cm$^3$. The gas jet, directed along the $x$ axis (perpendicular to the field propagation), is modeled in our code by a Gaussian distribution along the $y$ and $z$ dimensions (whose FWHM is 500 $\mu$m) and by a constant profile along its axial dimension, $x$ (the cylindrical symmetry is only in the polar integration for the maps).

## IV. CHARACTERIZATION OF THE DETECTION OF HIGH-ORDER HARMONICS DRIVEN BY APERTURED LASER BEAMS

To demonstrate the signature of the transversal coherence length, we have performed experiments on and theoretical computations of the variation of the harmonic yield as a function of the diameter of an apertured beam. This simple setup has been demonstrated to be useful to control various aspects relevant to phase matching: the Gouy phase, the intrinsic phase, and the free-charge density [20,21]. In their seminal paper [20], Kazamias *et al*. demonstrated that a middle-sized aperture was optimal to phase match the harmonics, giving rise to a factor-of-10 increase in the total harmonic yield. In that experiment, when aperturing, the variations in the phase-matching conditions can be attributed to changes in the Gouy phase gradient and in the density of free carriers. Therefore, the optimal aperture corresponds to the maximal compensation of these two contributions. Our experiment follows the same steps as Kazamias', but with the parameters changed in order to reduce the variations of all the main sources of phase mismatch (free charges, intensity gradient, Gouy-phase gradient) with the exception of the wavefront curvature radius. Therefore, we select a case in which aperturing affects mainly the transversal phase matching. To reduce the total ionization and the intensity gradient, our laser beam energy has been lowered (0.5 mJ, 100 fs instead of 6 mJ, 30 fs). We have chosen also a Gaussian smaller beam waist (4.5 mm in our case, vs the 11 mm in the Kazamias experiment) in order to reduce the clipping of the beam when the smallest aperture (4 mm) is used and, therefore, to reduce the change in the Gouy-phase gradient at the target when aperturing. We use a shorter focal length to obtain a similar Rayleigh length as in the Kazamias experiment, for our nonapertured beam. Briefly, we have designed our experiment so the effect of the aperture size in the longitudinal phase matching is minimal. As we see, the experiment still shows a pronounced variation in the harmonic generation efficiency with the aperture size. We, then, will use our numerical codes to demonstrate that this variation can only be attributed to the increase in the transversal coherence length.

In the simulations we have considered an 800-nm laser pulse and a 15.4-fs FWHM with the laser peak intensity at focus $2.5 \times 10^{14}$ W/cm$^2$. The laser pulse duration is shorter compared to that in experiments for computational reasons. However, as the ionization rates under the conditions presented here are very low, the same phase-matching conditions in the theory and the experiment are ensured by using the same laser intensity. We have modeled the experimental argon gas jet using the same distribution as in Fig. 1 with a 550-$\mu$m FWHM and a density of $10^{17}$ atoms/cm$^3$. The form of the apertured fundamental field is found by integrating the slowly varying envelope (SVEA) equation over the inhomogeneous gas target. The field found in this way is then used to compute the harmonic generation at the target. In Fig. 2 we represent the intensity (solid lines) and phase (dashed lines) of the fundamental field along the propagation axis, at a radius $\rho = 10$ $\mu$m [Fig. 2(a)], and along the radial axis, at (left) $-2$ mm and (right) 2 mm with respect to the focus position [Figs. 2(b)]. We performed simulations for a nonapertured laser beam (red lines) and laser beam (blue lines) apertured by a 10.5-diameter diaphragm. When the gas jet is centered at $-2$ mm, we observe that the variation of the Gouy phase

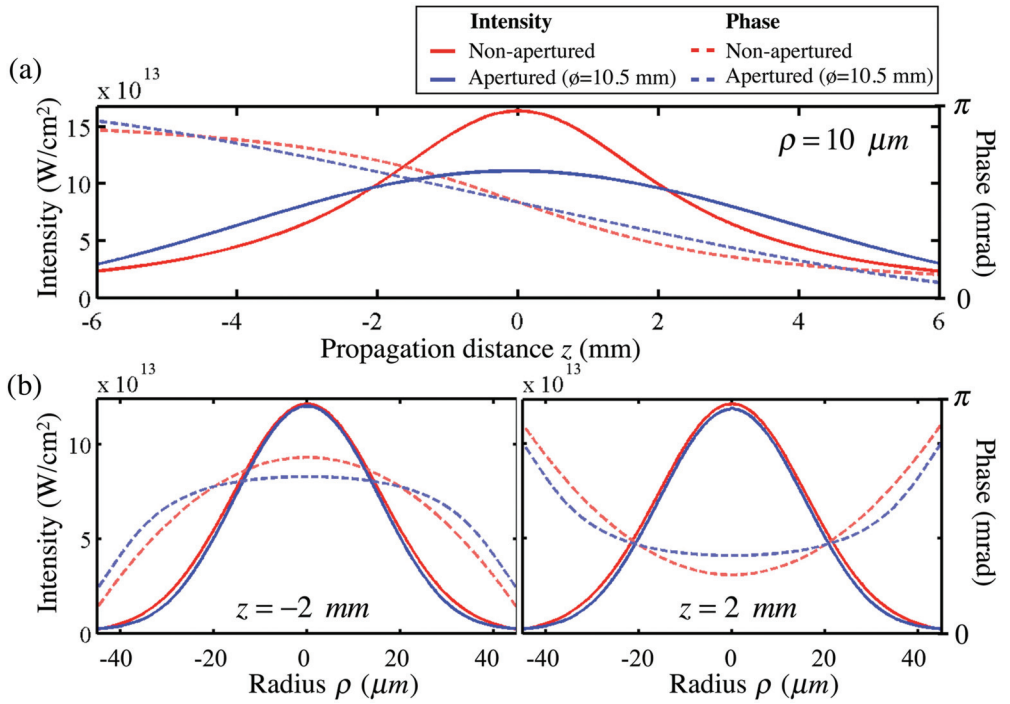


FIG. 2. (Color online) Intensity (solid lines) and phase (dashed lines) of the fundamental field, (a) along the propagation axis, at a radius $\rho = 10\ \mu$m, and (b) along the radial axis at (left) $-2$ mm and (right) 2 mm with respect to the focus position. We performed simulations for a nonapertured laser beam (red lines) and laser beam (blue lines) apertured by a 10.5-diameter diaphragm.

for the apertured and nonapertured beams remains similar. On the other hand, although there is a variation of the intensity gradient when aperturing, the absolute intensity is low, so the change in the intrinsic phase is small, a fact that can be checked from the numerical simulations. In addition, we observe that the gradient of the transversal phase is dramatically reduced when aperturing, thus increasing the transversal coherence length. As discussed before, the opposite sign of the transversal phase before the focus leads to the longer transversal coherence length. As a conclusion, from Fig. 2 we expect a small change in the longitudinal coherence length but a noticeable increase in the transversal when aperturing the laser beam.

In our experimental setup, odd harmonics of the fundamental frequency are generated by focusing the compressed laser beam (of about 0.5-mJ pulse energy) with a 40-cm-focal-length lens into a pulsed argon jet exiting from a 500-$\mu$m nozzle inside a vacuum chamber ($10^{-4}$ mbar). The laser peak intensity at focus is estimated to be $2.5 \times 10^{14}$ W/cm$^2$. The waist (radius) of the laser beam before the lens is 4.5 mm. The relative distance between the focus position and the gas jet is continuously changed using a motorized linear stage. In Fig. 3 we show the comparison of the transversal intensity profile of the fundamental laser beam when apertured with a diaphragm of 11.5 mm in diameter, recorded from the experiment, and computed with our SVEA code. The images were taken at three positions with respect to the focus ($\pm 0.1$, $\pm 0.3$, and $\pm 0.5$ mm). The agreement between the theoretical and the experimental profiles is excellent.

Once the XUV radiation was generated, a thin aluminum filter (150 nm thick) was used to eliminate the remaining infrared laser pulse. In the next step, the harmonics were spatially selected by a slit before being characterized by a Rowland circle-type XUV spectrometer (McPherson 248/310G) [22,23]. The spectrometer consists of a reflective spherical grating, a microchannel plate coupled to a phosphore screen, and a CCD detector, all of them inside a vacuum chamber ($10^{-6}$ mbar). In our measurements, the XUV radiation was angularly recorded in the CCD detector. This system was previously used to characterize the compression of ultraintense femtosecond pulses [24].

We have detected the harmonic signal for different iris diameters, from 7.5 mm to completely opened (16 mm). Measurements were obtained by integrating the 10-Hz signal over 8 min in the CCD detector. In Fig. 4 we show the detected harmonic signal for the 17th and 19th harmonics when the gas jet is placed at $-2$ mm [Figs. 4(a) and 4(e)], $-1$ mm [Figs. 4(b) and 4(f)], 1 mm [Figs. 4(c) and 4(g)], and 2 mm [Figs. 4(d) and 4(h)] with respect to the focus positions, respectively. Circles represent experimental results, whereas results of the HHG simulations computed using the fundamental field profile found in our SVEA calculations are represented by dashed (red) lines.

The agreement between theoretical and experimental results confirms that there is an optimal iris diameter for which the harmonic signal is higher, leading to an increase in the harmonic yield of a factor up to 8 compared to the nonapertured case (iris diameter of 16 mm). Also, as explained above, phase-matching conditions when the jet is located after or before the focus are different, therefore the enhancement turns out to be higher when the gas jet is placed before the focus. In any case, the existence of an optimal aperture is

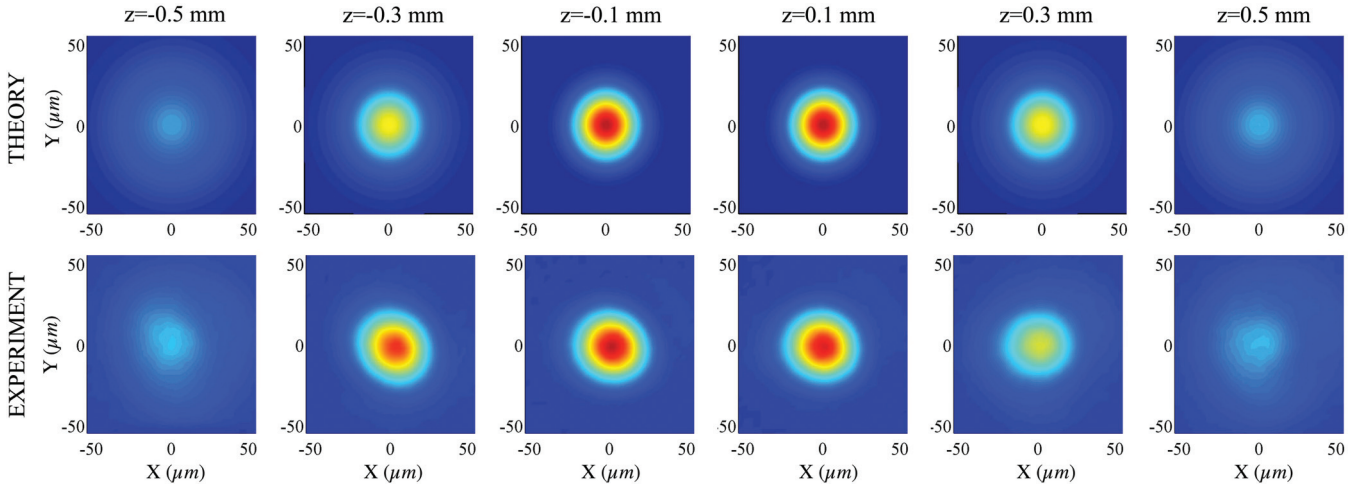


FIG. 3. (Color online) Transversal intensity profile—theoretical (top row) and experimental (bottom row)—of the laser beam apertured with a diaphragm 11.5 mm in diameter. The images were taken at three positions with respect to the focus (±0.1, ±0.3, and ±0.5 mm).

a surprising fact, since our laser parameters are chosen to minimize the effect of the aperture in all the phase-matching contributions that are usually considered (i.e., those affecting the longitudinal coherence length). In Fig. 5 we present the spatial maps of the 19th harmonic for a driving laser beam nonapertured [Figs. 5(a), 5(c), 5(e), and 5(g)] and apertured with a 10.5-mm iris diameter [Figs. 5(b), 5(d) 5(f), and 5(h)], for a gas jet placed at the same positions as in Fig. 4. This iris diameter corresponds to the one at which the detected signal in the experiment was optimal.

There are two main conclusions to be drawn from these maps. On one hand, while both transversal and longitudinal coherence lengths change when the laser beam is apertured, the change in the transversal coherence length is far more drastic. This is particularly evident when the gas jet is placed at ±2 mm, where the longitudinal coherence length associated with phase

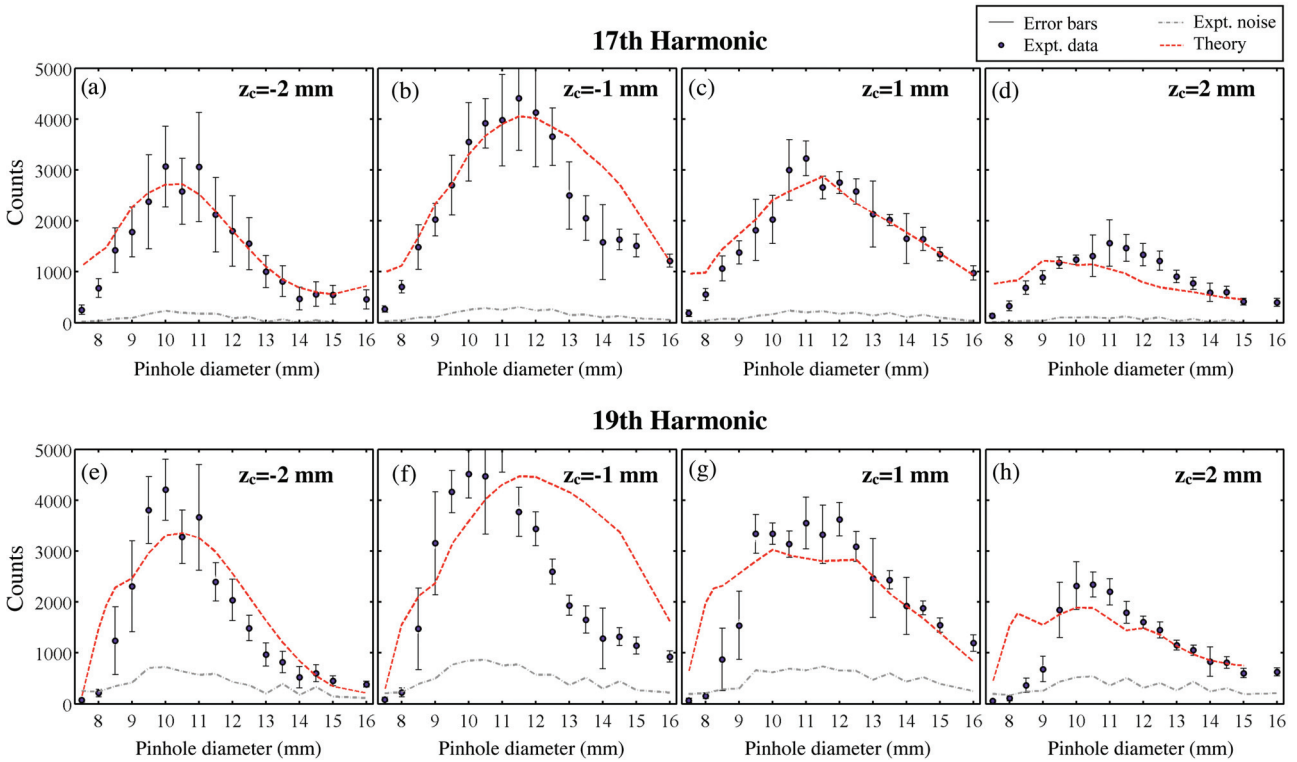


FIG. 4. (Color online) Detected signal versus iris diameter for (a)–(d) the 17th harmonic and (e)–(h) the 19th harmonic, for a gas jet placed (a) and (e) 2 mm before, (b) and (f) 1 mm before, (c) and (g) 1 mm after, and (d) and (h) 2 mm after the focus position. The experimental signal is represented by black circles and error bars; the background noise, by the lower dashed (gray) line. Simulations [dashed (red) line] use a laser pulse of 15.4-fs FWHM and 0.5-mJ total energy. The argon gas jet is modeled as a Gaussian function of 550 $\mu$m in the propagation direction, with a density of $10^{17}$ atoms/cm$^3$.

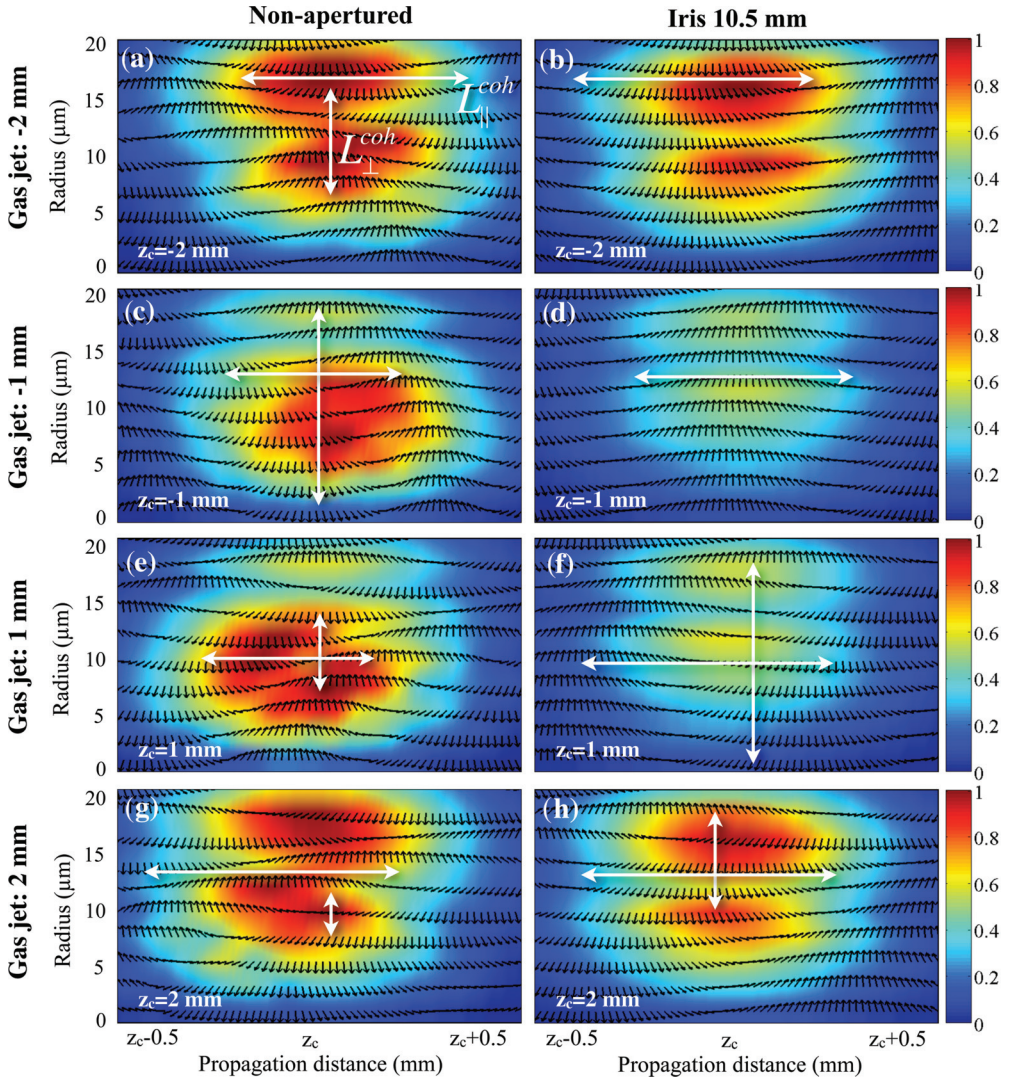


FIG. 5. (Color online) Spatial maps of the detected 19th harmonic for a driving laser beam (a), (c), (e), and (g) unapertured and (b), (d), (f), and (h) apertured with a 10.5-mm iris diameter, for a gas jet placed at (a) and (b) −2 mm, (c) and (d) −1 mm, (e) and (f) 1 mm, and (g) and (h) 2 mm with respect to the focus position. Simulation parameters are the same as in Fig. 4, where the nonapertured laser beam corresponds to an iris diameter of 16 mm. Longitudinal and transversal coherence lengths are represented as white horizontal and vertical arrows. Note that in (b) and (d) the transversal coherence length is not indicated, as it is longer than the radial interval represented. The color scales (in arbitrary units) are chosen to compare the apertured and non-apertured laser beam cases at the particular positions of the gas jet, therefore, they are the same for each target position (i.e., among the columns along the same row), while renormalized at every target position (i.e., form row to row), to enhance visibility.

matching remains very similar (horizontal white arrows), as expected from our parameter choice. As a consequence, the higher yield of the apertured beam cannot be attributed to the optimization of the longitudinal phase matching, as was the case in the Kazamias *et al.* experiment [20]. Our simulations demonstrate that the enhancement of the yield wwith aperturing is a direct consequence of the transversal coherence length. Secondly, as explained in Sec. II, this effect is more acute before the focus, where the transversal coherence length is larger. This behavior can also be observed in our simulations and experimental results: the increase of the transversal coherence length before the focus [Fig. 5(a) to 5(b)], is higher than after the focus [Fig. 5(g) to 5(h)] and is reflected in substantially higher enhancement of the experimental signal when the gas jet is placed at −2 mm than 2 mm respect to the focus position [see Figs. 4(e) and 4(h)].

On the other hand, if we move the target towards the focus (positions ±1 mm), the longitudinal coherence length also plays an important role when aperturing. Both transversal and longitudinal phase matching are relevant and thus the enhancement is due to these two factors.

## V. CONCLUSION

We have demonstrated, with an experiment and corresponding theoretical support, the signature of a transversal coherence length in the harmonic emission of a macroscopic target. By aperturing the laser beam in HHG we have demonstrated experimental conditions under which phase -matching cannot

be understood in terms of just the longitudinal coherence length. With the aid of spatial maps of HHG, the macroscopic signatures of phase matching have been unequivocally attributed to the transversal coherence length.

## ACKNOWLEDGMENTS

We acknowledge technical support from Oscar Varela, Juan Hernández Toro, and Cruz Méndez. We acknowledge support by a Marie Curie International Outgoing Fellowship within the EU Seventh Framework Programme for Research and Technological Development, under REA Grant Agreement No. 328334. We acknowledge support from Junta de Castilla y León (Consejería de Educación and Fondo Social Europeo and Projects No. SA002B08 and No. SA116U13), Spanish MINECO (Grant No. FIS2009-09522, Consolider Program SAUUL CSD2007-00013, and Ramón y Cajal Program), and Centro de Láseres Pulsados, CLPU.

[1] K. J. Schafer, B. Yang, L. F. DiMauro, and K. C. Kulander, Phys. Rev. Lett. **70**, 1599 (1993).
[2] P. B. Corkum, Phys. Rev. Lett. **71**, 1994 (1993).
[3] M. Lewenstein, Ph. Balcou, M. Yu. Ivanov, A. L'Huillier, and P. B. Corkum, Phys. Rev. A **49**, 2117 (1994).
[4] A. Zaïr, M. Holler, A. Guandalini, F. Schapper, J. Biegert, L. Gallmann, U. Keller, A. S. Wyatt, A. Monmayrant, I. A. Walmsley, E. Cormier, T. Auguste, J. P. Caumes, and P. Salières, Phys. Rev. Lett. **100**, 143902 (2008).
[5] A. L'Huillier, K. J. Schafer, and K. C. Kulander, Phys. Rev. Lett. **66**, 2200 (1991).
[6] P. Salières, A. L'Huillier, and M. Lewenstein, Phys. Rev. Lett. **74**, 3776 (1995).
[7] T. Popmintchev, M. Chen, P. Arpin, M. M. Murnane, and H. C. Kapteyn, Nature Photon. **4**, 822 (2010).
[8] M. Kretschmar, C. Hernández-García, D. S. Steingrube, L. Plaja, U. Morgner, and M. Kovačev, Phys. Rev. A **88**, 013805 (2013).
[9] M. Lewenstein, P. Salières, and A. L'Huillier, Phys. Rev. A **52**, 4747 (1995).
[10] P. Antoine, A. L'Huillier, and M. Lewenstein, Phys. Rev. Lett. **77**, 1234 (1996).
[11] P. Balcou, P. Salieres, A. L'Huillier, and M. Lewenstein, Phys. Rev. A **55**, 3204 (1997).
[12] J. Peatross, M. V. Fedorov, and K. C. Kulander, J. Opt. Soc. Am. B **12**, 863 (1995).
[13] C. Hernández-García, J. A. Pérez-Hernández, J. Ramos, E. C. Jarque, L. Roso, and L. Plaja, Phys. Rev. A **82**, 033432 (2010).
[14] A. L'Huillier, X. F. Li, and L. A. Lompré, J. Opt. Soc. Am. B **7**, 527 (1990).
[15] A. L'Huillier, P. Balcou, S. Candel, K. J. Schafer, and K. C. Kulander, Phys. Rev. A **46**, 2778 (1992).
[16] J. A. Pérez-Hernández, L. Roso, and L. Plaja, Opt. Express **17**, 9891 (2009).
[17] J. A. Pérez-Hernández, C. Hernández-García, J. Ramos, E. Conejero Jarque, L. Plaja, and L. Roso, *New Methods For Computing High-Order Harmonic Generation and Propagation*, Springer Series in Chemical Physics, Vol. 100 (Springer, New York, 2011), Chap. 7, p. 145.
[18] C. Hernández-García and L. Plaja, J. Phys. B: At. Mol. Opt. Phys. **45**, 074021 (2012).
[19] L. E. Chipperfield, P. L. Knight, J. W. G. Tisch, and J. P. Marangos, Opt. Commun. **264**, 494 (2006).
[20] S. Kazamias, F. Weihe, D. Douillet, C. Valentin, T. Planchon, S. Sebban, G. Grillon, F. Augé, D. Hulin, and Ph. Balcou, Eur. Phys. J. D **21**, 353 (2002).
[21] A. Dubrouil, Y. Mairesse, B. Fabre, D. Descamps, S. Petit, E. Mevel, and E. Constant, Opt. Lett. **36**, 2486 (2011).
[22] J. L. Schwob, A. W. Wouters, S. Suckewer, and M. Finkenthal, Rev. Sci. Instrum. **58**, 1601 (1987).
[23] B. J. MacGowan, J. A. Koch, and S. Mrowka, Rev. Sci. Instrum. **63**, 5122 (1992).
[24] C. Hernández-García, C. Méndez, I. Arias, J. R. Vázquez de Aldana, O. Varela, I. J. Sola, and L. Roso, Appl. Phys. B **108**, 773 (2012).